Experimental Mechanics (2024) 64:1107–1121
https://doi.org/10.1007/s11340-024-01080-y

RESEARCH PAPER

Optimizing Pure Shear Experiment to Properly Characterize the Shear Properties of Thin-Walled Aluminum Alloy Tubes

S. Zhang[1] · X. Wang[1,2] · W. Hu[3] · G. Liu[1,2]

Received: 18 September 2023 / Accepted: 8 May 2024 / Published online: 30 May 2024

Abstract

Background For an anisotropic thin-walled tube without changing its circular geometry, only the experimental data of initial yield and subsequent plastic deformation along the axial and circumferential directions can be obtained till now. These experimental data are not sufficient to construct an anisotropic constitutive relation for simulations of tube deformation processes.

Objective A novel shear test of tubular materials is proposed to achieve the state of shearing plastic deformation along the axial direction of thin-walled tubes.

Methods Two semi-circle mandrels and one specially designed tubular specimen are used in the shear experiment. Optimizations of the specimen shape and mandrel structure were carried out by using FE simulation. The inf luence of the specimen shape, such as the length of the shear zone and the length of the axial slot, on the stress state of the shear zone was discussed. A thin-walled 5052 aluminum tube was used in the shear experiment using the optimized specimen shape. To understand the corresponding relationship between the tensile properties and the shear properties of an anisotropic tube, the uniaxial tension stress-strain relationship was equivalently transformed to the shear stress-stain relationship using the Mises, Tresca, Hill48, and Barlat-lian constitutive functions.

Results After optimizing the specimen shape, the shearing condition of the tested tube is closer to the pure shear stress state. Based on the tests, the pure shear stress state can be maintained to a large deformation extent. The experimental shear stress-strain relationship was compared with the converted stress-strain relationship based on the uniaxial tension tests using the Mises, Tresca, Hill48, and Barlat-lian constitutive functions. The results show a large difference between the transformed stress-strain relationship and the shear stress-strain relationship.

Conclusions This testing method can provide necessary empirical data with the principal stress directions along the direction at an angle of 45° to the tube axis. The shear plastic deformation properties of some anisotropic materials cannot be equivalently described by the experimental data of the tensile test. The shearing characteristics obtained by this novel experimental method can be applied to the characterizations of anisotropic constitutive relations for simulations of tube deformation processes.

Keywords Thin-walled tube · Pure shear · Shear stress-strain relationship · Aluminum alloy

Nomenclature

F	Tensile force
T	Torque caused by the two parallel force
σ_2	Second principal stress
t	Real-time tube thickness
D	Outer diameter of the tube
L_s	Length of the axial slot
$F_{upper-A}$	Counterforce from upper semi-circle mandrel to half-tube A
σ_z	Normal stress along the axial direction of the tube
$\tau_{\theta z}$	The shear stress along the axial direction of the tube
σ_{z0}	The yield stress in the axial direction
R_z	R-value in the axial direction
$\overline{\sigma}$	The equivalent stress
$\overline{\Delta\epsilon}$	The increment of the equivalent strain

✉ X. Wang
hitxswang@hit.edu.cn

[1] School of Materials Science and Engineering, Harbin Institute of Technology, Harbin, China

[2] National Key Laboratory of Precision Hot Processing of Metals, Harbin Institute of Technology, Harbin, China

[3] Research Institute of Baosteel, Shanghai, China

$\tau_{\theta z0}$	The shear yield stress obtained in the axial shear experiment
ρ,ξ, λ, δ	Parameters used in Hill48 constitutive function
F_z	Compressive force acting on the end plane (perpendicular to the tube axis) of each half-tube
σ_1	First principal stress
σ_3	Third principal stress
L	Real-time length of the shear zone
τ	Shear stress
$F_{lower-A}$	Counterforce from lower semi-circle mandrel to half-tube A
$F_{lower-B}$	Counterforce from lower semi-circle mandrel to half-tube B
σ_θ	Normal stress along the circumferential direction of the tube
$\tau_{z\theta}$	The shear stress along the circumferential direction of the tube
$\sigma_{\theta 0}$	The yield stress in the circumferential direction
R_θ	R-value in the circumferential direction
σ_b	Equal-biaxial tensile stress
σ_{45}	Yield stress along the 45° direction to the rolling direction of the sheet
$\Delta\gamma$	Increment of the shear strain
a, c, q	Coefficients of Barlat-Lian constitutive function

Introduction

Tubes involved in the deformation processes are generally manufactured by rolling, extrusion, and drawing. It would lead to the mechanical properties of such tubes to exhibit anisotropic characteristics. If a constitutive relation is used to simulate a tube deformation process, the experimental data involving the anisotropic properties of the formed tube must be considered to meet the prediction accuracy. But to date, only the experimental data along a tube's axial and circumferential directions can be obtained, including the simplest approach of the uniaxial tension test using a cambered specimen, the ring hoop tension test, and tube bulging experiments [1–5]. However, all the experimental characteristics are based on normal stress, and the principal axis is along the axial and circumferential direction, which belong to the same principal coordinate.

Similar to characterizing the anisotropic plastic deformation characteristics of rolled sheet metals, i.e., the experimental data of a uniaxial tension along 45° direction to the rolling (RD) is usually needed to identify the constitutive parameters, it is essential to find the second principal coordinate to build the anisotropic constitutive relation for simulations of formed tubes.

Trying to apply shearing experimental data of the formed tubes involving the principal stress directions along a non-axial and circumferential direction of a tube to define a constitutive relation should be another effective method. Free-end torsion and combined axial-torsion loading are often used to achieve the shear loading of thin-walled tubes [6–9]. However, these experiments cannot provide sufficient data for characterizing a constitutive relation for numerical simulations because these tests cannot maintain the direction of principal stress steady along the desired direction in the loading process with large deformation. It should be pointed out that the pure shear state is discussed in some research work on the calibration of constitutive functions using tubes loaded with axial force and internal pressure[5, 10, 11]. This kind of pure shear stress state is caused by the axial compressive stress and circumference tensile stress, which have the same absolute stress value. However, it is not a real shear deformation as the axial stress and circumferential stress are both normal stress.

A new pure shear test for thin-walled tubes that overcomes these shortcomings will be beneficial for describing the deformation behavior of anisotropic tubes. Mechanical property testing methods for thin-walled tubes are always carried out and referred to as those for sheet metals. There are three representative shear tests for sheet, e.g., a simple shear test proposed by Miyauchi [12], the well-known test setup based on the American Society for Testing and Materials standard ASTM B831 [13], and the twin bridge torsion shear test reported by Brosius et al. [14]. The three shear tests are commonly conducted using a translational movement, and the specific regions will be deformed by shear deformation.

A limitation of these sheet shear tests is that the shear deformation often accompanies the normal stress. To avoid instability and maintain deformation in the designed deformation zone, the shear test device has to contain two clamping structures to make the material move parallel to each other. Because of the influence of the constraint of the clamping areas, normal stress occurs inevitably. Previous analyses of the in-plane shear test results commonly neglected the occurrence of normal stress components [15–18]. However, some numerical studies have reported that the normal stress components can reach magnitudes similar to shear stress [19]. If there aren't clamping structures, the material in the shear zone tends to rotate with large deformation, which means the direction of principal stress is not steady along the desired direction.

Following up on the principle of translational movement, we introduced a novel shear test for thin-walled tubes in this paper. This test can create a steady pure shear stress state in the center zone of a tubular specimen. Specimen shapes were analyzed to reduce the heterogeneity of stress and strain distribution. Differences in the stress-strain relationships between the one obtained from the uniaxial tension test and the one obtained from the shear test proposed herein

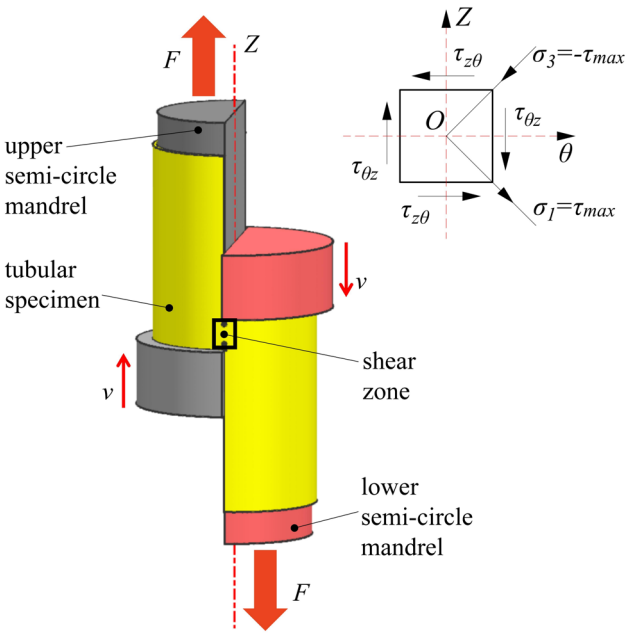

Fig. 1 Working principle of the shear test

are compared and analyzed. This test makes the experimental data of tubes for the second principal axes available and enables the construction of a realistic anisotropic constitutive relation for thin-walled tubes.

Principle of Pure Shear Loading of Tubes and Design of Experimental Device

The working principle of the novel shear device of thin-walled tubes is illustrated in Fig. 1. The device used in these tests comprises a specially designed tubular specimen and two semi-circle mandrels. The testing specimen is cut from a tube. Half of the tube is removed at two opposite ends while the center zone of the specimen remains intact. The mandrel is a scalar semi-circle cylinder. The diameter of the smaller semi-circle cylinder is the same as the inner diameter of the tube. In comparison, the diameter of the larger semi-circle cylinder is larger than the outer diameter of the tube. The two semi-circle mandrels are placed inside the tubular specimen, and a tensile force parallel to the tube axis is applied to the ends with the smaller diameter for both mandrels. One mandrel is loaded at the upper half-tube, and the other is loaded at the lower half-tube. Because the tensile force is applied separately to each half-tube of the specimen, the specimen will tend to rotate. With the support of the two semi-circle mandrels, the tubular specimen can only move along the axial direction. Thus, only a shear deformation occurs in the center zone of the tubular specimen, i.e., the connection zone of the two half-tubes.

The stress state of the center zone of the shear zone is also shown in Fig. 1, where the first principal stress is equal to the maximum shear stress, and the angle between the first principal stress and the axis of the tube is 45°. The second principal stress is equal to zero. The magnitude of the third principal stress is equal to the maximum shear stress, but this stress is negative. The angle between the third principal stress and the axis of the tube is -45°.

1. Shear stress calculation.

   The acting region of the shear stress is the interface plane of the two half-tubes through the axis of the tube. The tensile force F is measured using the force sensor

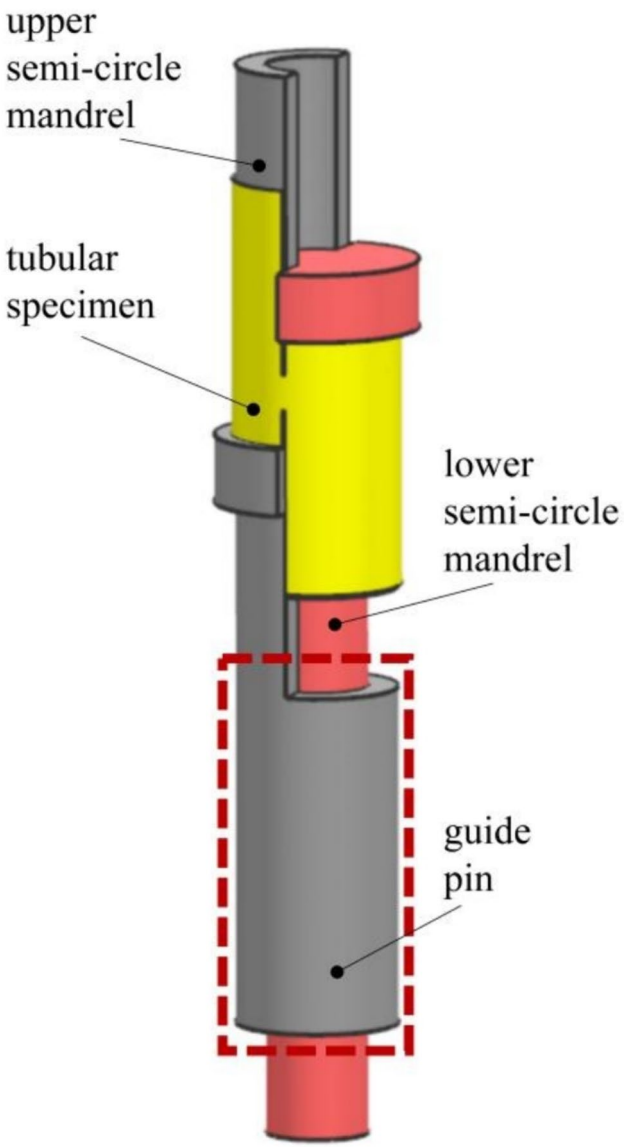

Fig. 2 Guide pin structure for the two mandrels to improve the stability of the shear test

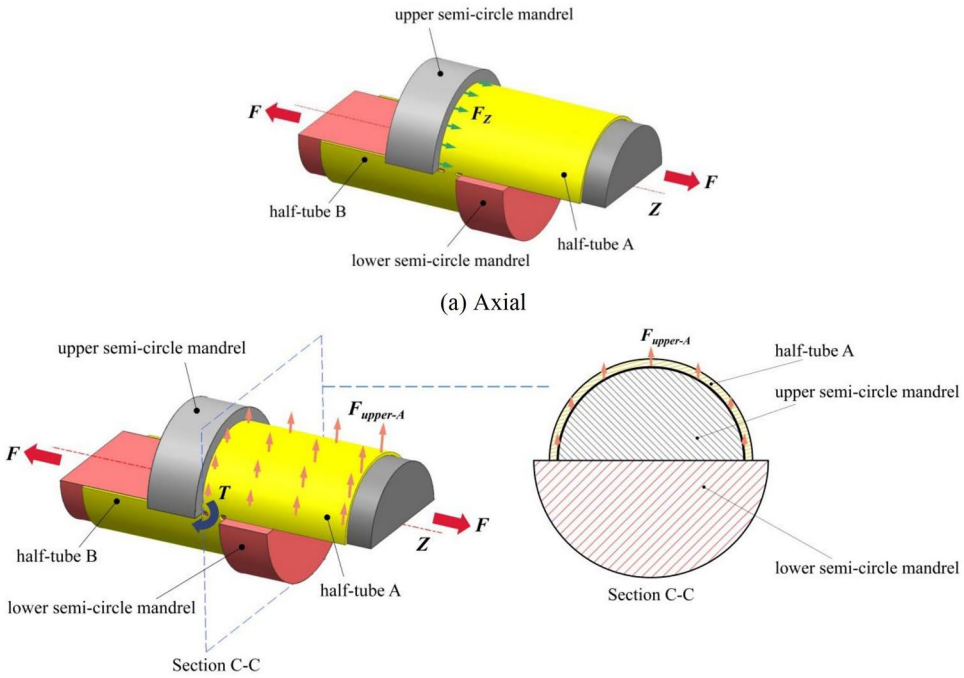

Fig. 3 Force diagram of the specimen

of the testing machine. Shear stress can be calculated according to equation (1).

$$\tau = \frac{F}{2 \times L \times t} \tag{1}$$

where τ is the real-time average shear stress, F is the force required to deform the two shear zones, L is the real-time length of the shear zone, and it decreases with increasing deformation, D is the outer diameter of the tube, and t is the real-time tube thickness. Strain is measured using a three-dimensional digital image correlation (DIC) system.

As the corresponding semi-circle mandrel and the half-tube move together, there is no friction force between them. The friction force only exists between the interface plane of the two semi-circle mandrels, so the friction force should be counted when calculating the shear stress.

2. Measures to prevent rotation of the mandrels.

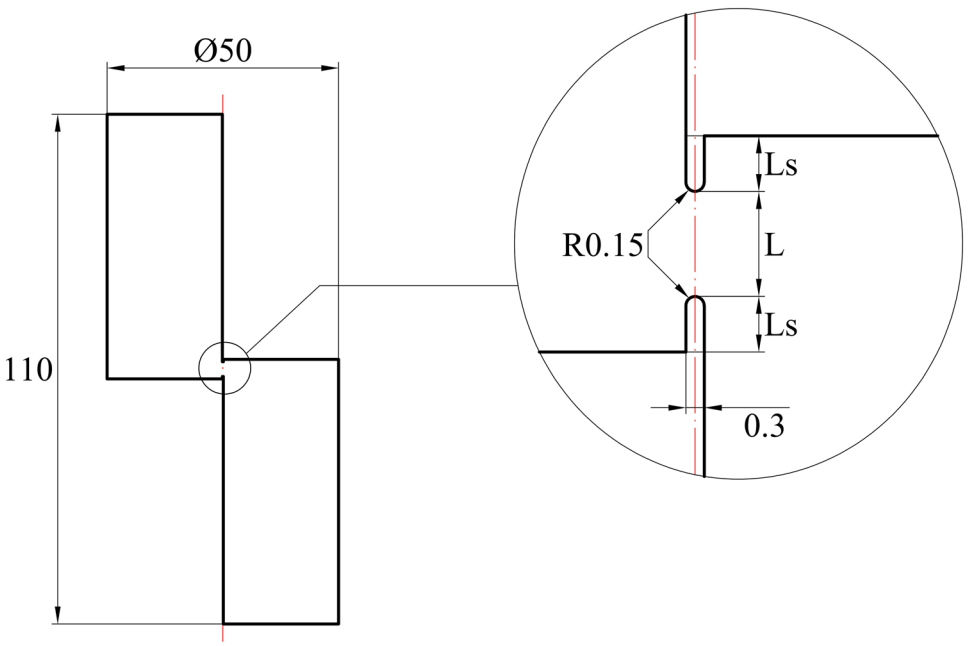

Fig. 4 Dimension of the specimen (unit: mm)

Table 1 Simulation scheme

Variables	Length of the slot along the axial direction/tube thickness (L_s/t)	Length of the shear zone/ tube thickness (L/t)
Value	1, 2.5, 4	2.5, 4, 5.5

There exists a rotation tendency of two mandrels as two parallel forces are added to two mandrels. To ensure the movement of the two mandrels strictly along the tube axis, two concentric cylinders are added to the ends of the two semi-circle mandrels on the same side as the guide pin used in the stamping die, as shown in Fig. 2. Deformation is more concentrated in the pre-set shear zone with the guiding mandrel structure, the stability of shear deformation is improved [20].

Stress and Strain Distribution Homogeneity with FEM Simulation

Simulation Model

To achieve a pure shear stress state, finite element simulations are conducted to obtain the optimized specimen shape. These factors below are considered to obtain the proper specimen dimensions. As the two half-tubes are under the same loading state, only half-tube A is discussed below.

1. Axial Stress

   For this method, the translational movement of the two half-tubes is caused by the compressive force F_z acting on the end plane (perpendicular to the tube axis) of each half-tube along the axial direction, as shown in Fig. 3(a). Increasing the shear zone length means greater compressive force on the end plane of the half-tube, which will make the axial normal stress bigger. If the value of the normal stress on the end plane of the half-tube is too high, the pure shear stress state will be strongly perturbed. So, the length of the shear zone should not be too long.

   Long and thin slots are set to the two ends of the specimen's shear zone to ensure a certain distance between the end plane and the shear zone. Thus, the axial normal stress in the shear zone is much smaller than that on the end plane. Meanwhile, if the length is too small, strain measurement error will increase, disturbing the results.

2. Circumferential stress

   The two parallel compressive forces act on the specimen, which causes a torque T to make the specimen rotate, as shown in Fig. 3(b). As the rotation of the specimen was hindered by the semi-circle mandrels, there will be a counterforce from the part of the semi-circle mandrel with a small diameter to the half-tubes of the specimen along the normal direction of the interface plane of the two half-tubes.

The semi-circle mandrels are named upper semi-circle mandrel and lower semi-circle mandrel, while the two half-tubes are named half-tube A and half-tube B. The counterforce from the upper mandrel to half-tube A is called $F_{upper\text{-}A}$, and the counterforce from the lower mandrel to half-tube B is called $F_{lower\text{-}B}$, the two forces balance the torque together. The direction of the counterforce $F_{upper\text{-}A}$ is the normal direction of the interface plane of the two half-tubes, thus it causes circumferential stress in the shear zone. Suppose the length of the half-tube is much longer than the length of the shear zone. In that case, the action area of the counterforce is larger, and the distance between the action area and the shear zone is larger, so the circumferential stress can be reduced to a minimum, which helps maintain the pure shear stress state.

Considering the above factors comprehensively, the dimension of the specimen is shown in Fig. 4. The length of the specimen is much larger than the length of the shear zone. The shear zone length L and the axial slot length L_s are to be decided from the simulation. The width of the axial slot is set as 0.3 mm, which is the minimum length that the wire-electrode cutting operation can machine.

As the shear deformation is under the plane stress and the plane strain state, the shear specimen is meshed with shell elements (S3 and S4R) in ABAQUS/Standard. To save the calculation time, the element edge length in the shear zone and the shell element thickness are set as 0.1 mm. The element size is a little bit large for the 0.15 mm radius of the axial slot but is enough for the deformation zone. Isotropic elastic-plastic material behavior, according to the

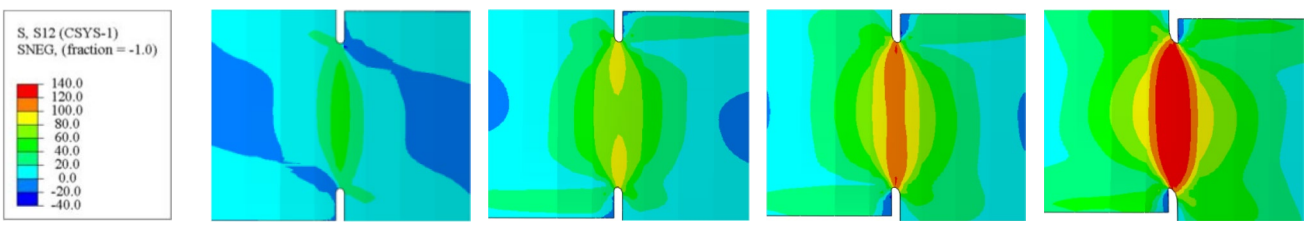

(a) 0.002 (b) 0.05 (c) 0.1 (d) 0.3

Fig. 5 Nephogram of shear stress distribution with different shear strain of the center point (L_s/t = 1, L/t = 4)

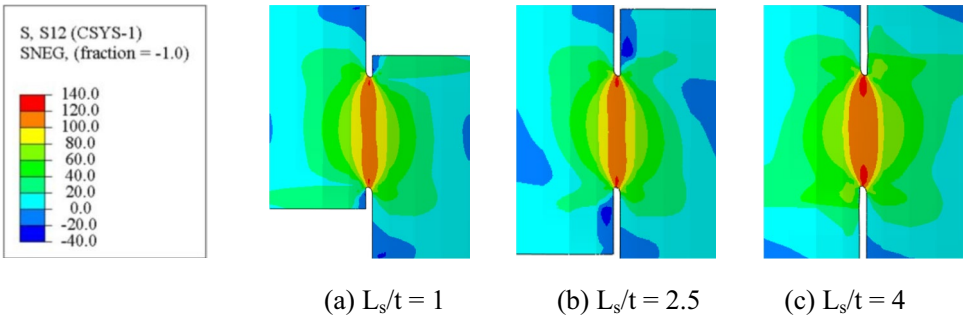

Fig. 6 Nephogram of shear stress distribution with different L_s/t ratios (shear strain of the center point equals 0.12)

Mises criterion, is used. The flow curve used for the input of the numerical simulation is extrapolated from the result of a uniaxial tension test along the axial direction of the tube. In the simulation, one-half of the tube is loaded with a specific axial displacement. At the same time, the other half is fixed to realize the axial shear deformation of the tube specimen. The two semi-circle mandrels are set to move along the axis of the tube, and there is no constraint for the specimen. The gap between the inner surface of the tube and the mandrel is set to 0.05 mm, the same as in the experiment. Simulation is carried out according to Table 1. The friction coefficient between the two semi-circle mandrels is set as 0.2.

As the elements at the two ends of the shear zone are severely distorted at larger strain and fracture is not considered in the used material model, the maximum shear strain is set as 0.3. The simulation can no longer describe the specimen behavior at this deformation stage.

Influence of the Length of the Axial Slot Along the Axial Direction on Stress Homogeneity

The length of the shear zone L is four times the thickness in this section. The nephogram of shear stress distribution is shown in Fig. 5 when the L_s/t ratio is set as 1. It is shown that the deformation of the specimen is concentrated at the interface of the two half-tubes, i.e., the pre-set shear zone. Shear stress at the two ends of the deformation zone increases fast initially, then the stress distribution in the interface plane becomes even.

The nephogram of shear stress distribution with different L_s/t ratios is shown in Fig. 6 when the shear strain of the center point equals 0.12. For the L_s/t ratio equals 1 and 2.5 (Fig. 6(a) and (b)), the shear strain at the two ends of the shear zone is bigger than the shear strain of the center point, and the shear strain is relative even distributed along the interface of the two half-tubes. For the L_s/t ratio equals 4 (Fig. 6(c)), the shear strain at the two ends of the shear zone

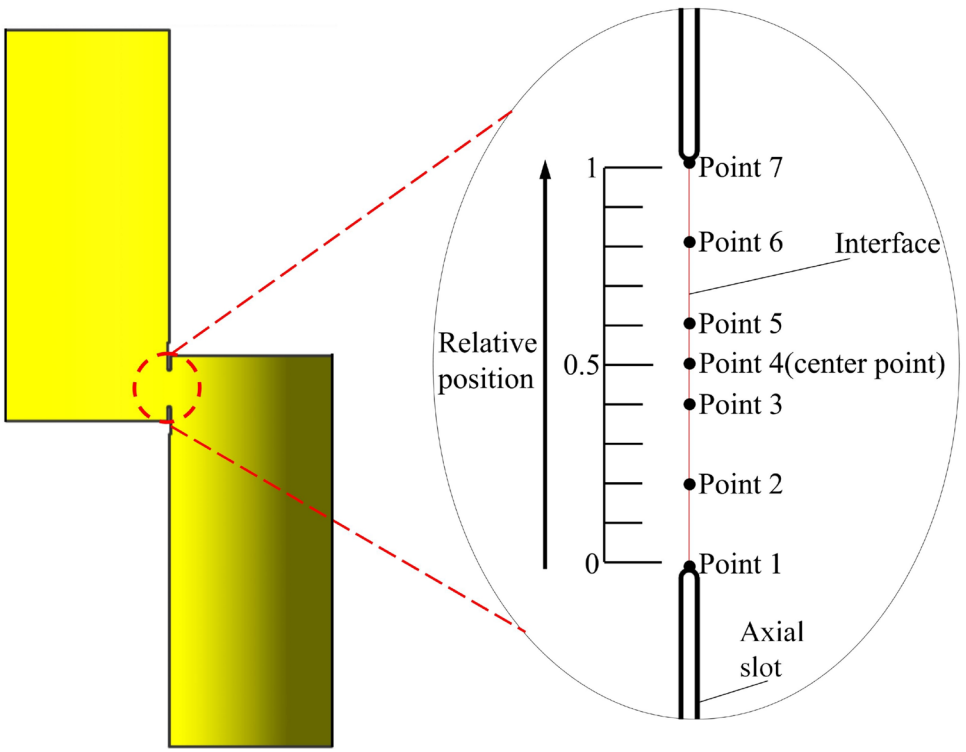

Fig. 7 Location of the representative points

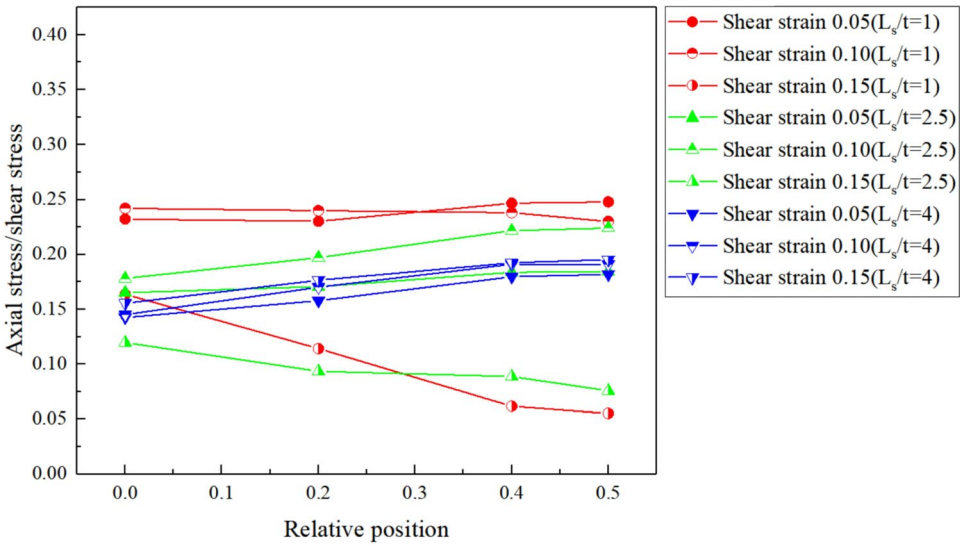

(a) Axial stress/shear stress

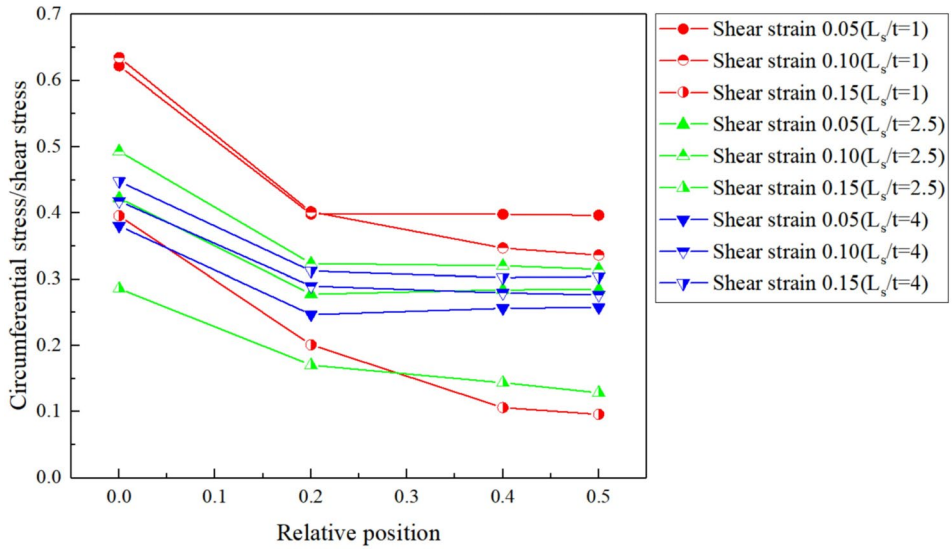

(b) Circumferential stress/shear stress

Fig. 8 Ratio of axial/circumferential stress to shear stress along the interface of the shear zone

is much bigger than the shear strain of the center point, and the uniformity of the stress distribution is lowered.

Seven representative points, as shown in Fig. 7, are chosen to investigate the stress state. The seven points are located in the interface of the two half-tubes. Point 4 is the center point, while point 1 is at one end of the shear zone.

The ratio of the axial/circumferential stress to shear stress along the interface of the shear zone, when the shear strain of the center point equals 0.05, 0.10, and 0.15, is

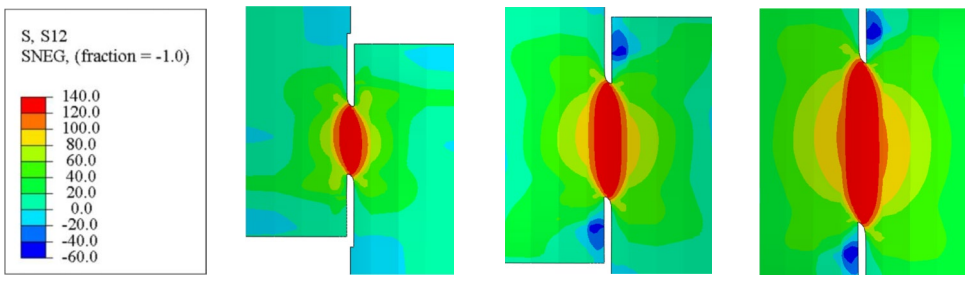

(a) L/t=2.5 (b) L/t=4 (c) L/t=5.5

Fig. 9 Nephogram of shear stress of the shear zone for different L/t values

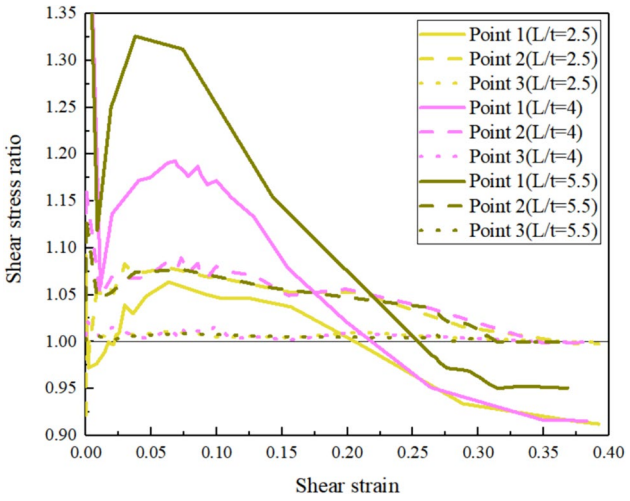

Fig. 10 Relationship of shear stress ratio between representative points and center point with shear strain of the center point

shown in Fig. 8. Ratio of axial stress to shear stress is about 0.1–0.25 for all L_s/t values. This ratio of L_s/t equals 2.5 or 4 is smaller than that of $L_s/t = 1$. The ratio of circumferential stress to shear stress is bigger than that of the axial stress to shear stress. For L_s/t equals 2.5 or 4, the ratio is also smaller than L_s/t equals 1. The value is more even for L_s/t equals 2.5, so this value is chosen to conduct the simulation in the following section.

Influence of the Length of the Shear Zone L

As shear stress can only be calculated according to the load and the real-time length of the shear zone, it is an average value. In this section, the influence of the length of the shear zone on stress homogeneity is analyzed. The L_s/t value is set as 2.5.

The nephogram of shear stress for different shear zone lengths when the shear strain of the center point equals 0.3 is shown in Fig. 9. It can be seen that shear deformation is concentrated in the pre-set zone, i.e., the interface of the two half-tubes.

The ratio of the shear stress of the representative points to that of the center point is used to evaluate the stress homogeneity. The relationship between the shear stress ratio and the shear strain of the center point(point 4) is shown in Fig. 10. With the increase of the L/t value, the shear stress ratio for points 1, 2, and 3 increased, which means the shear stress homogeneity decreased. For the L/t value equals 2.5, the shear stress ratio is closer to 1. This L/t value is chosen in the following simulation.

Influence of Torque-balanced Zone

The proper axial slot length and shear zone length were obtained through the simulation results carried on the original specimen shape shown in Fig. 4. However, it can be seen

Fig.11 The counterforce from the lower semi-circle mandrel to the half-tube A

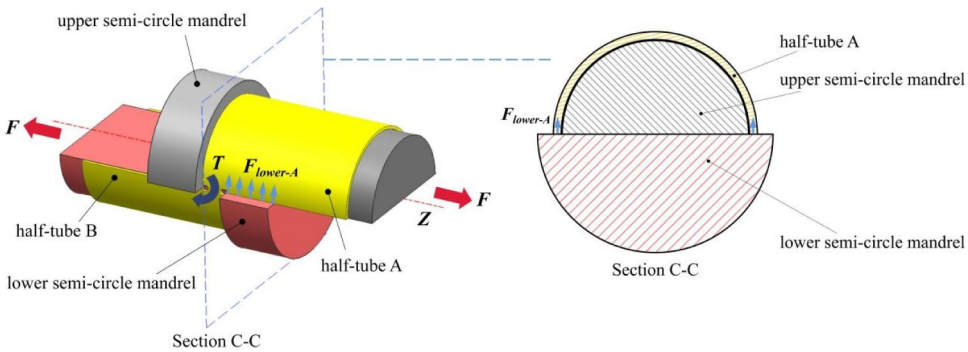

(a) Counterforce from the lower semi-circle mandrel to the half-tube A

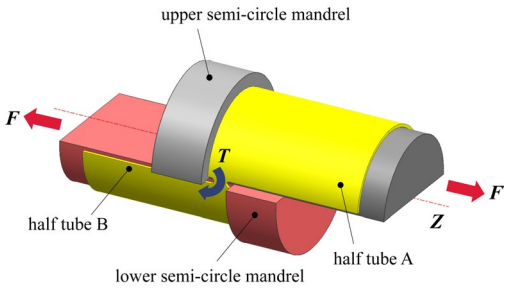

(b) Modified specimen to eliminate the counterforce $F_{lower\text{-}A}$

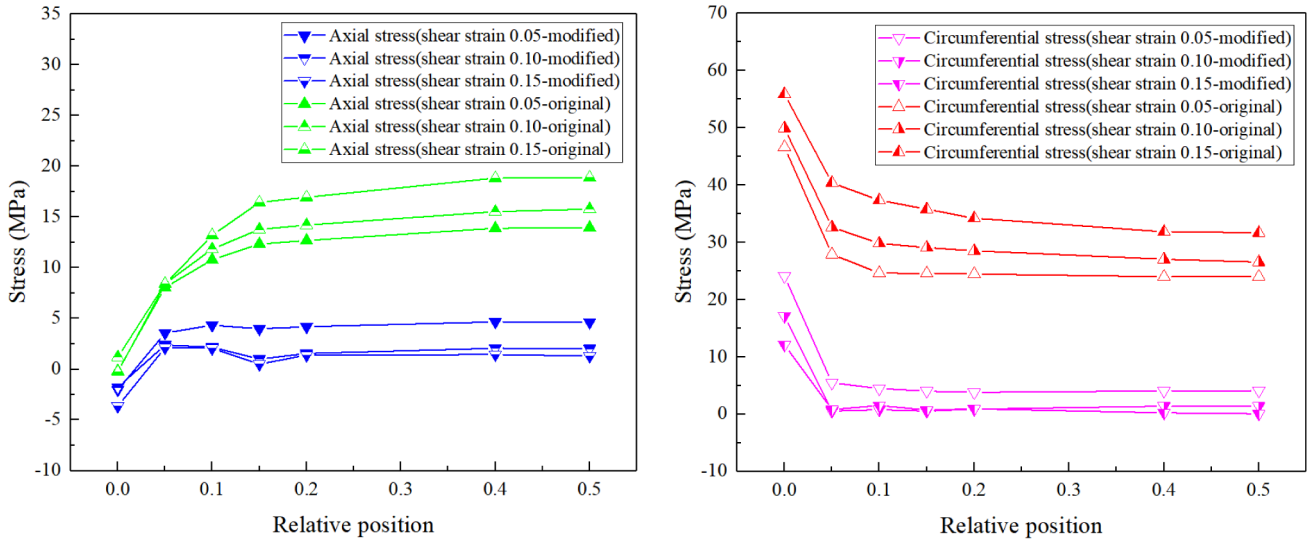

(a) Axial stress (b) Circumferential stress

Fig. 12 Normal stress distribution along the axial direction for the original specimen and modified specimen

from Fig. 8(b) that the circumferential stress is relatively high, as it is about 0.3–0.5 times the shear stress.

It has been discussed that the counterforce from the upper semi-circle mandrel to half tube A caused the circumferential stress in the shear zone, as shown in Fig. 3(b). In fact, for the original shape specimen, there is also a counterforce from the lower semi-circle mandrel to the half tube A, which is named $F_{lower\text{-}A}$, as shown in Fig. 11(a). Further, as the action zone of $F_{lower\text{-}A}$ is adjunct to the shear zone, the influence of the counterforce on the stress state, especially on the circumferential stress, cannot be ignored. To eliminate the counterforce $F_{lower\text{-}A}$, the specimen shape is modified to make the half-tube A uncontacted with the lower semi-circle mandrel, as shown in Fig. 11(b). Simulation is carried out to investigate the influence of the shape modification on the stress states.

To accurately obtain the stress state of the endpoint of the deformation zone, the element size is set as 0.02 mm in the successive simulation. Meanwhile, because the stress value difference between the endpoint(point 1) and the neighboring point (point 2) is large, several representative points between the two points are chosen to investigate the stress state of this area.

The axial and circumferential stress distribution of representative points along the axial direction with different shear strains at the center point is shown in Fig. 12.

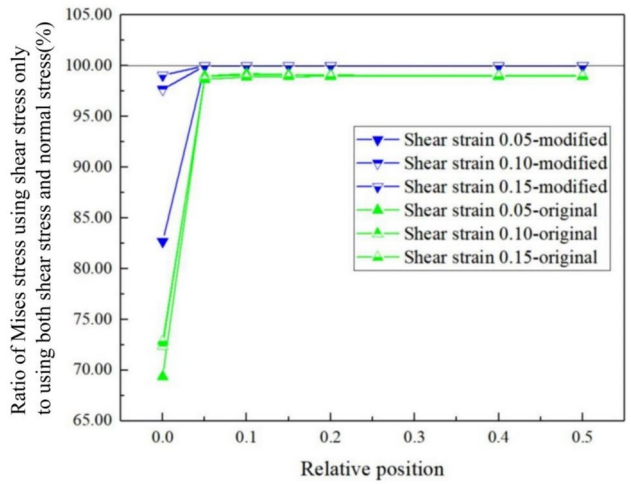

Fig. 13 Ratio of Mises equivalent stress between using shear stress only and using normal stress and shear stress

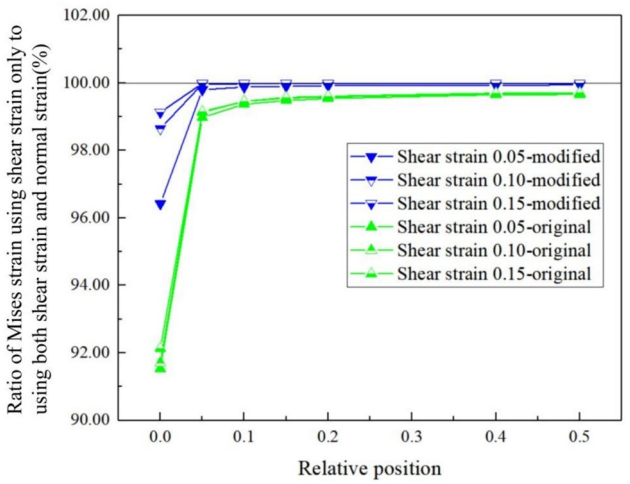

Fig. 14 Ratio between Mises strain using shear strain only and using both normal strain and shear strain

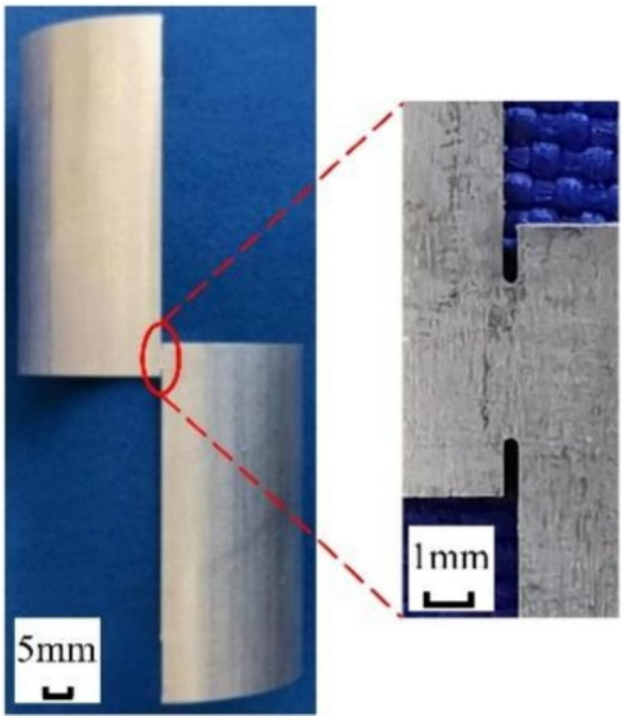

Fig. 15 Tubular specimen for the pure shear test (L/t = 2.5)

Both axial stress and circumferential stress of the modified specimen are smaller than that of the original specimen, especially for circumferential stress at the end of the shear zone.

Mises equivalent stress is calculated using shear stress only or both normal and shear stress. The ratio of the two kinds of equivalent stress is shown in Fig. 13. The influence of the shear stress in deformation is more significant when the ratio is closer to 1. The ratio at the endpoint for the original shape specimen is only 69%. In contrast, it is about 82% for the modified shape specimen, which means that the influence of normal stress at the endpoint is still considerable. In other areas of the deformation zone, the ratio is 98% for the original shape specimen and nearly 100% for the modified specimen. It is indicated that the stress state is very close to the pure shear stress state for the modified specimen.

Similar to the calculation of Mises stress, Mises strain is calculated using shear strain only or both normal and shear strain for the original and modified specimen. The ratio of Mises strain between using shear strain only and using both normal and shear strain for different points is shown in Fig. 14.

The strain calculation results are also similar to that of the Mises stress. The proportion of the shear strain is smaller at the endpoint of the deformation zone for the original and modified specimen. The proportion of the shear strain is higher for the modified specimen than for the original specimen. It is indicated that the deformation for the modified shape specimen can be regarded as pure shear deformation.

Shear Experiment of a Thin-walled Aluminum Tube

Material and Dimension of the Specimen

An annealed thin-walled 5052 aluminum tube with an outer diameter of 50 mm and a nominal thickness of 1.2 mm was used in the experiment. The tubular specimen is shown in Fig. 15. According to the optimized result, the ratio of axial slot length to thickness L_s/t and the ratio of shear zone length to thickness L/t are both set as 2.5.

The length of the shear zone and the thickness of the specimen were measured for each specimen. There are two shear planes for one specimen; the areas of the two shear planes are calculated using the length and the thickness, and the shear zone with a smaller area was measured by the DIC system. The diameter of the combined two semi-circular mandrels was measured to calculate the gap between the inner surface of the tubular specimen and the circular mandrel. Two specimens were tested. The dimensions of the two specimens are shown in Table 2.

Table 2 Dimensions of the specimens (in mm, unless specified otherwise)

No.	Inner diameter	Shear plane A			Shear plane B			Gap
		Thickness	Length of the shear zone	Area /mm^2	Thickness	Length of the shear zone	Area /mm^2	
1	47.60	1.20	3.00	3.60	1.20	3.01	3.61	0.05
2	47.60	1.20	2.99	3.59	1.20	3.00	3.60	0.05

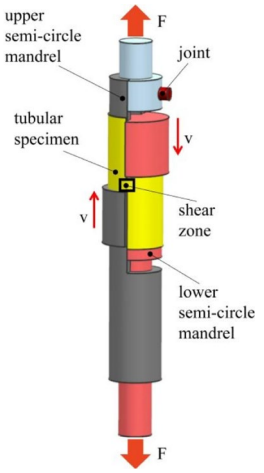

(a) Schematic diagram

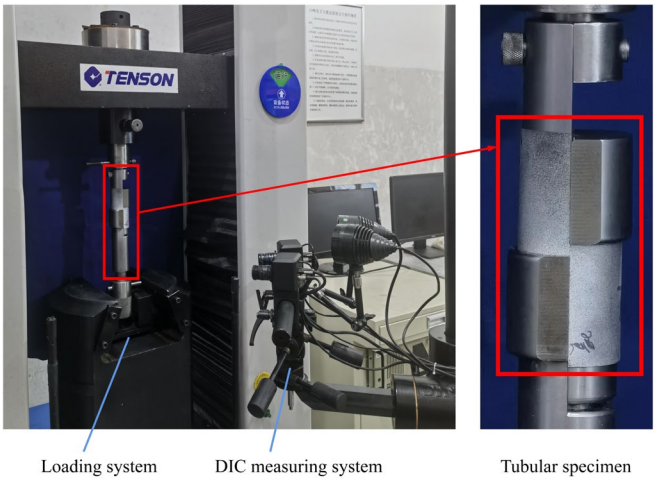

(b) Experimental equipment

Fig. 16 Experimental device used for the pure shear test

Experimental Setup

The shear experiments were carried out using a WDW-T200 tension machine at HIT (Harbin Institute of Technology). A schematic illustration of the assembly testing device is shown in Fig. 16(a), and the testing device and its enlarged view are shown in Fig. 16(b). The tensile speed was set to 1 mm/min, which leads to a shear strain rate of 0.001 s^{-1}. A lubricant was used between the contact surfaces of the two semi-circle mandrels to decrease the friction force between the two mandrels. The friction force between the two semi-circle mandrels was tested without the specimen, and the force was less than 10N, so it would not disturb the calculation of the shear stress.

A three-dimensional digital image correlation (DIC) system developed by Xi'an Jiaotong University was used for the strain measurement.

The cracked specimen is shown in Fig. 17. The shear fracture occurred along the axial direction, and the two shear zones cracked at the same time for both specimens.

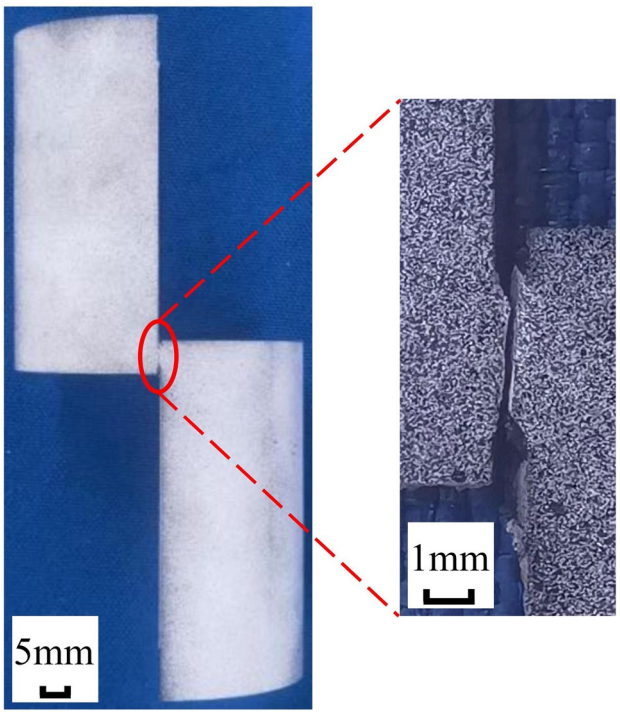

Fig. 17 Cracked specimen (L/t = 2.5)

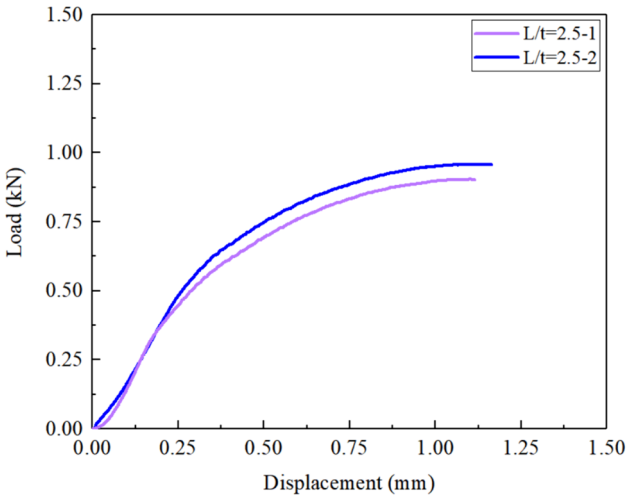

Fig. 18 Relationship between the loading force and displacement

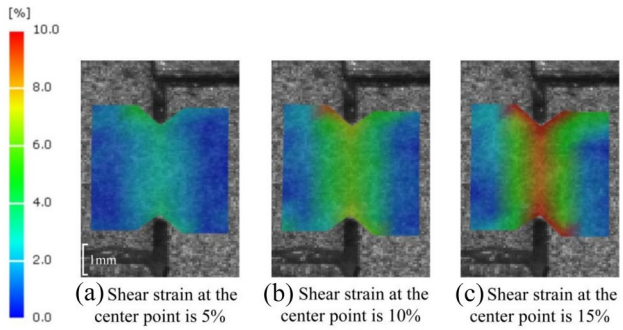

Fig. 19 Distribution of Mises equivalent strain (L/t = 2.5)

Results and Discussion

Load-Displacement Relationship and Experimental Strain Distributions

The relationship between the axial tensile force and displacement is shown in Fig. 18. The endpoint of each curve means the time of the crack. The difference between the loading relationship of two specimens with the same shear zone length is minimal.

The Mises equivalent strain distribution is shown in Fig. 19. It can be seen that deformation begins with the two ends of the shear zone, and then deformation extends to the center zone. The width of the shear zone with a higher equivalent strain is about 1 mm, which means deformation is highly concentrated in the interface plane of the two half-tubes.

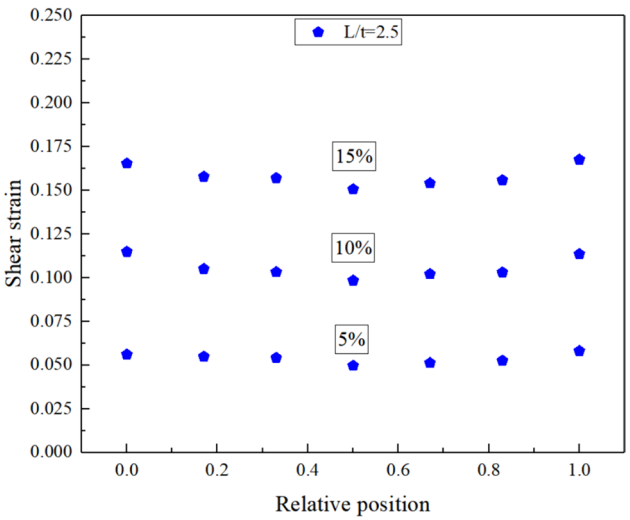

Fig. 20 Distribution of the shear strain in the interface plane along the tube axis (the shear strain of the center point equals 5%, 10%, and 15%)

The shear strain distribution along the interface plane is shown in Fig. 20. The horizontal ordinate is the relative position. The minimum shear strain is located in the center point. It should be noted that the shear strain distribution is symmetrical, which indicates nearly no rotation occurs for the two semi-circle mandrels. As the shear stress is an average value and only the shear strain of one point in the shear zone can be used in the shear stress-strain relationship, the specimen with a more even shear strain distribution will be closer to the actual shear stress-strain relationship. Though the shear strain in the two ends is bigger than that of the center point, the shear strain distribution for specimens with L/t = 2.5 is relatively even.

Shear strain distribution in the surface of the shear zone is shown in Fig. 21. The X and Y coordinates are the axial and circumferential distance separately, and the Z coordinate is the shear strain value. The zero point for the circumferential direction is the interface of the two half-tubes. Furthermore, the zero point for the axial direction is the center of the shear zone. It can be seen that the shear strain is symmetrically distributed about the interface of the two half-tubes. The maximum shear strain value along the circumferential direction lies in the interface. The shear strain is decreased with increased distance from the interface. This means the shear deformation is highly concentrated in the pre-set shear plane, i.e., the interface plane. Thus, the shear stress value calculated using the load and the area of the interface is closer to the actual value, and the precision of the shear stress is improved.

Prediction of Constitutive Relation

Generally, simulation models used in engineering applications do not consider the shear experimental properties of materials. That is to say, the shear properties of materials are generally equivalently represented by the tensile experimental properties of materials. However, due to the influence of anisotropic properties of materials, it is necessary to understand whether the shear properties of anisotropic materials can be approximately described by tensile experimental properties.

For a plane-stress anisotropic model, typical calibration experiments involve tensile tests in three orientations relative to the rolling direction of the sheet and an equal-biaxial test with each test providing both stress and R-value. The parameters are σ_0, σ_{45}, σ_{90}, σ_b, R_0, R_{45}, R_{90}.

For the thin-walled tubes, σ_z denotes the axial normal stress, σ_θ denotes the circumferential normal stress, $\tau_{\theta z}$ denotes the shear stress along the axial direction. The

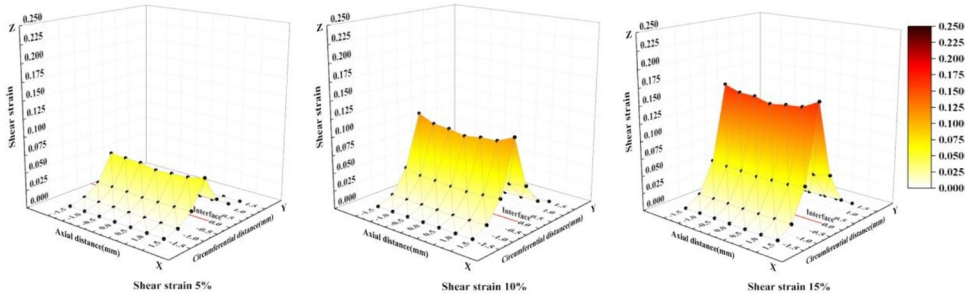

Fig. 21 Distribution of the shear strain (the shear strain of the center point equals 5%, 10%, and 15%)

(a) Shear strain equals 5% (b) Shear strain equals 10% (c) Shear strain equals 15%

yield stress is set as the Mises equivalent strain equals 0.2%. σ_{z0} and $\sigma_{\theta 0}$ are the yield stress in the axial and circumferential directions, where R_z and R_θ are R-values in the axial and circumferential directions, respectively. $\tau_{\theta z0}$ is the shear yield stress. The experimental results are shown in Table 3.

The σ_{45} value is not available for tubes, and the equal-biaxial tensile stress σ_b cannot obtained using a general tension machine, so the two stress values are estimated using the axial and circumferential properties using equations (2) and (3).

$$\sigma_{45} = \frac{\sigma_{z0} + \sigma_{\theta 0}}{2} \tag{2}$$

$$\sigma_{\mathrm{b}} = \frac{\sigma_{z0} + \sigma_{\theta 0}}{2} \tag{3}$$

The constitutive models are calibrated using the results of the uniaxial tension tests above. The uniaxial tension stress is converted to shear stress using the constitutive functions. Then, the shear strain is calculated according to the criterion of equal first-order incremental work, as shown in equation (4).

$$\overline{\sigma}\Delta\overline{\varepsilon} = \tau\Delta\gamma \tag{4}$$

Mises, Tresca, Hill48, and Barlat-lian constitutive function are used to carry out the equivalent conversion, and the stress-strain relationship obtained from the uniaxial tension test using the cambered specimen along the axial direction is used in the conversion.

The Barlat-Lian constitutive function is shown as equation (5), where M = 8 for FCC materials. The equivalent stress is shown as equation (6), while the detailed description can be found in reference [21]. The coefficients used in the calculation of the equivalent stress of the constitutive function are shown in Table 4.

$$\mathrm{f} = \mathrm{a}|\mathrm{k}_1 + \mathrm{k}_2|^{\mathrm{M}} + \mathrm{a}|\mathrm{k}_1 - \mathrm{k}_2|^{\mathrm{M}} + \mathrm{c}|2\mathrm{k}_2|^{\mathrm{M}} = 2\overline{\sigma}^{\mathrm{M}} \tag{5}$$

$$-\sigma = \sqrt[M]{\frac{2a + 2^M c}{2}} q\tau_{\theta z} \tag{6}$$

The relationship between the shear stress and equivalent stress is shown in equation (7)

$$\overline{\sigma} = 1.653\tau_{\theta z} \tag{7}$$

The Hill48 constitutive function and the equivalent stress equation are shown in equations (8) and (9), respectively [22]. Hill's coefficients can be calculated directly from the anisotropy coefficients.σ_b is yield stress in biaxial tension and is calculated according to equation (3).

$$f = \sigma_z^2 - \left(\frac{\sigma_{z0}^2}{\sigma_{\theta 0}^2} - \frac{\sigma_{z0}^2}{\sigma_b^2} + 1\right)\sigma_z\sigma_\theta + \frac{\sigma_{z0}^2}{\sigma_{\theta 0}^2}\sigma_\theta^2 + F\tau_{\theta z}^2 = \overline{\sigma}^2 \tag{8}$$

$$\overline{\sigma} = \sqrt{\rho\sigma_z^2 + \xi\sigma_\theta^2 + \lambda(\sigma_z - \sigma_\theta)^2 + 2\delta\tau_{\theta z}^2} \tag{9}$$

Table 3 Experimental characteristics of thin-walled 5052 aluminum alloy tube

Test	Yield stress (MPa)	R-values
Uniaxial tension along axial direction using the camber specimen	$\sigma_{z0} = 72.44$ MPa	$R_z = 0.615$
Ring hoop tension test	$\sigma_{\theta 0} = 65.15$ MPa	$R_\theta = 0.572$
Pure shear test along the axial direction	$\tau_{\theta z0} = 43.83$ MPa	-

Table 4 Coefficients used in calculation of the equivalent stress of Barlat-Lian

a	c	q
1.256	0.744	0.934

Table 5 Coefficients used in the calculation of the equivalent stress of Hill48

Parameter	ρ	ξ	λ	δ
Value	0.436	0.672	0.563	1.663

The coefficients of the Hill48 constitutive function are shown in Table 5, and the relationship between the shear stress and equivalent stress is shown in equation (10)

$$\overline{\sigma} = 1.824\tau_{\theta z} \tag{10}$$

The stress-strain relationships predicted using the Mises, Tresca, Hill48, and Barlat-lian constitutive functions are shown in Fig. 22(a), and the relative error is shown in Fig. 22(b). The Barlat-Lian and Mises functions underestimate the shear stress at the initial stage, and both overestimate the shear stress at the subsequent stage. For the Tresca and Hill48 functions, the shear stress is always underestimated. It can be seen that the precision of all of the predictions is not good.

As the equal-biaxial tensile stress σ_b is not obtained from the experiment, the σ_b value is enlarged or lessened to investigate its influence on prediction precision. When the equal-biaxial tensile stress σ_b equals 0.9 or 1.1 times the calculated average value of σ_{z0} and $\sigma_{\theta 0}$, the equation is shown as equations (11) and (12).

When $\sigma_b = 0.9 * (\frac{\sigma_{z0}+\sigma_{\theta 0}}{2})$,

$$\overline{\sigma} = 1.750\tau_{\theta z} \tag{11}$$

When $\sigma_b = 1.1 * (\frac{\sigma_{z0}+\sigma_{\theta 0}}{2})$,

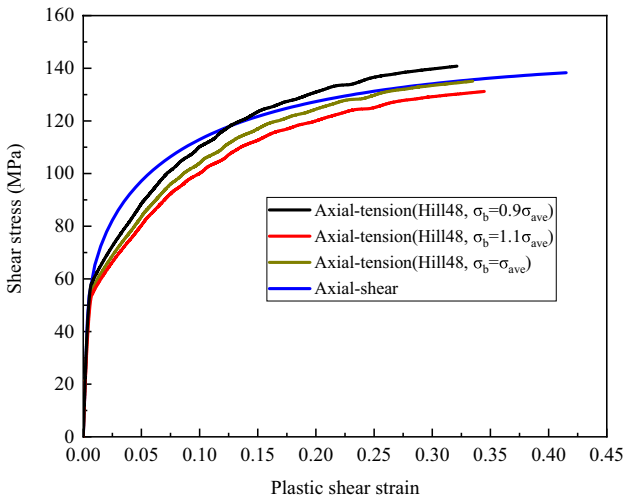

Fig. 23 Influence of the equal-biaxial tensile stress on prediction of shear stress-strain relationship of Hill48 constitutive function

$$\overline{\sigma} = 1.878\tau_{\theta z} \tag{12}$$

The predicted results are shown in Fig. 23. The predicted shear stress decreased with the increased value of the equal-biaxial tensile stress. However, the prediction precision is not improved with the change of the equal-biaxial tensile stress.

It is indicated that predictions of the models calibrated with the conventional method are inconsistent with the mechanics of shear deformation described in the shear experiment. In other words, the work hardening of the materials under a shear stress state does not appear to be the same as for uniaxial tension.

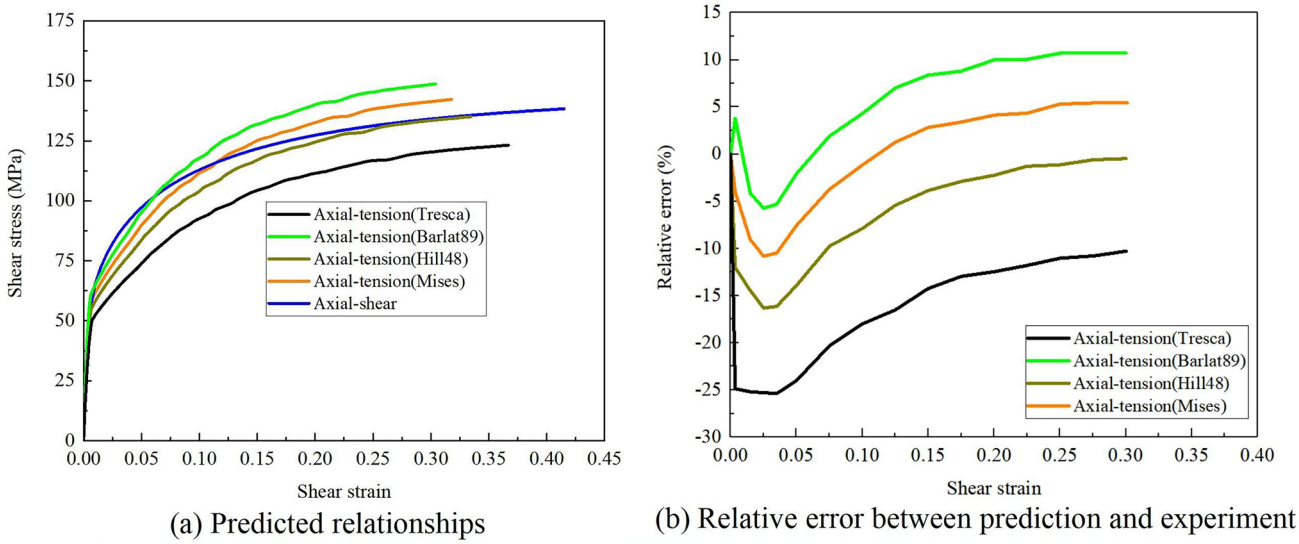

(a) Predicted relationships

(b) Relative error between prediction and experiment

Fig. 22 Predicted shear stress-strain relationships by different constitutive functions

Summary and Conclusions

A novel testing method and associated device are proposed to achieve pure shear deformation along the axial direction of a thin-walled tube. Optimizations of the specimen shape and experimental device were carried out by using FE simulation. Moreover, it was verified by a shear experiment of a thin-walled aluminum tube. Based on the tests, the pure shear stress state can be maintained to a large deformation extent. The experimental shear stress-strain relationship was compared with the converted stress-strain relationship based on the uniaxial tension tests using the Mises, Tresca, Hill48, and Barlat-lian constitutive functions. A significant difference between the stress-strain relationships is found. This indicates that the uniaxial tension stress-strain relationship cannot accurately predict shear deformation.

The shearing characteristics obtained by this novel experimental method can be applied to the construction of anisotropic constitutive relations for simulations of tube deformation processes. This testing method can provide necessary empirical data with the principal stress directions along the direction at an angle of 45° to the tube axis. The advantage of this pure shear loading method is that the shearing deformation occurs in a fixed two-dimensional shearing plane rather than in a three-dimensional shear zone, as previous studies of shear experiments considered.

Funding This work was financially supported by the National Natural Science Foundation of China (Project Number: 51975147). The authors would like to take this opportunity to express their sincere appreciation.

Data Availability The raw/processed data required to reproduce these findings cannot be shared at this time as the data also forms part of an ongoing study.

Declarations

Conflict of Interest On behalf of all authors, the corresponding author declares that there are no known competing financial interests or personal relationships that could have appeared to influence the work reported in this paper.

References

1. Bae BK, Cho SK, Seok CS (2008) A study on ring tensile specimens. Mater Sci Eng A 483–484:248–250
2. Dick CP, Korkolis YP (2014) Mechanics and full-field deformation study of the Ring Hoop Tension Test. Int J Solids Struct 51:3042–3057
3. Hwang YM, Wang CW (2009) Flow stress evaluation of zinc copper and carbon steel tubes by hydraulic bulge tests considering their anisotropy. J Mater Process Tech 209:4423–4428
4. Shirayori A, Fuchizawa S, Ishigure H, Narazaki M (2003) Deformation behavior of tubes with thickness deviation in circumferential direction during hydraulic free bulging. J Mater Process Tech 139:58–63
5. Wang XS, Hu WL, Huang SJ, Ding R (2019) Experimental investigations on extruded 6063 aluminium alloy tubes under complex tension-compression stress states. Int J Solids Struct 168:123–137
6. Yoshida K, Ishii A, Tadano Y (2014) Work-hardening behavior of polycrystalline aluminum alloy under multi-axial stress paths. Int J Plast 53:17–39
7. Sung SJ, Liu LW, Hong HK, Wu HC (2011) Evolution of yield surface in the 2D and 3D stress spaces. Int J Solids Struct 48:1054–1069
8. Khan AS, Kazmi R, Pandey A, Stoughton T (2009) Evolution of subsequent yield surfaces and elastic constants with finite plastic deformation. Part-I: A very low work hardening aluminum alloy (Al6061-T6511). Int J Plast 25:1611–1625
9. Kabirian F, Khan AS (2015) Anisotropic yield criteria in τ-s stress space for materials with yield asymmetry. Int J Solids Struct 67–68:116–126
10. He ZB, Zhang K, Zhu HH, Lin YL, Fu MW, Yuan SJ (2022) An anisotropic constitutive model for forming of aluminum tubes under both biaxial tension and pure shear stress states. Int J Plast 152:103259
11. Hu Q, Yoon JW, Chen J (2023) Analytically described polynomial yield criterion by considering both plane strain and pure shear states. Int J Plast 162:103514
12. Miyauchi K (1984) A proposal of a planar simple shear test in sheet metals. Sci Pap Inst Phys Chem Res (Jpn) 78:27–40
13. ASTM B769-11 (2005) Test method for shear testing of thin aluminum alloy products. ASTM. Int
14. Brosius A, Yin Q, Güner A, Tekkaya AE (2011) A new shear test for sheet metal characterization. Steel Res Int 82:323–328
15. Bouvier S, Haddadi H, Lev'ee P, Teodosiu C (2006) Simple shear tests: Experimental techniques and characterization of the plastic anisotropy of rolled sheets at large strains. J Mater Process Tech 172:96–103
16. Yin Q, Zillmann B, Suttner S, Gerstein G, Biasutti M, Tekkaya AE et al (2014) An experimental and numerical investigation of different shear test configurations for sheet metal characterization. Int J Solids Struct 51:1066–1074
17. Kohar CP, Bassani JL, Brahme A, Muhammad W, Mishra RK, Inal K (2019) A new multi scale framework to incorporate microstructure evolution in phenomenological plasticity: theory, explicit finite element formulation, implementation and validation. Int J Plast 117:122–156
18. Yoon JW, Barlat F, Gracio JJ, Rauch E (2005) Anisotropic strain hardening behavior in simple shear for cube textured aluminum alloy sheets. Int J Plast 21:2426–2447
19. Pereira AG, Prates PA, Oliveira MC, Fernandes JV (2019) Normal stress components during shear tests of metal sheets. Int J Mech Sci 164:105169
20. Wang XS, Zhang SN, Liu G (2023) Influence of mandrel guide structure on axial shear loading for thin-walled tubes. Forging & Stamping Technology 48(5):221–226 (in Chinese)
21. Kang JD, Wilkisnon DS, Wu PD, Bruhis M, Jain M, Embury JD, Mishra RK (2008) Constitutive Behavior of AA5754 Sheet Materials at Large Strains. J Eng Mater 130:031004
22. Carbonniere J, Thuillier S, Sabourin F, Brunet M, Manach PY (2009) Comparison of the work hardening of metallic sheets in bending–unbending and simple shear. Int J Mech Sci 51:122–130